Amplitude Mode in Quantum Magnets via Dimensional Crossover

Chengkang Zhou,[1] Zheng Yan,[1,2] Han-Qing Wu,[3] Kai Sun,[4,*] Oleg A. Starykh,[5,†] and Zi Yang Meng[1,‡]
[1]Department of Physics and HKU-UCAS Joint Institute of Theoretical and Computational Physics, The University of Hong Kong, Pokfulam Road, Hong Kong SAR, China
[2]State Key Laboratory of Surface Physics and Department of Physics, Fudan University, Shanghai 200438, China
[3]School of Physics, Sun Yat-Sen University, Guangzhou 510275, China
[4]Department of Physics, University of Michigan, Ann Arbor, Michigan 48109, USA
[5]Department of Physics and Astronomy, University of Utah, Salt Lake City, Utah 84112, USA

(Received 31 July 2020; revised 15 December 2020; accepted 3 May 2021; published 1 June 2021)

We investigate the amplitude (Higgs) mode associated with longitudinal fluctuations of the order parameter at the continuous spontaneous symmetry breaking phase transition. In quantum magnets, due to the fast decay of the amplitude mode into low-energy Goldstone excitations, direct observation of this mode represents a challenging task. By focusing on a quasi-one-dimensional geometry, we circumvent the difficulty and investigate the amplitude mode in a system of weakly coupled spin chains with the help of quantum Monte Carlo simulations, stochastic analytic continuation, and a chain-mean field approach combined with a mapping to the field-theoretic sine-Gordon model. The amplitude mode is observed to emerge in the longitudinal spin susceptibility in the presence of a weak symmetry-breaking staggered field. A conventional measure of the amplitude mode in higher dimensions, the singlet bond mode, is found to appear at a lower than the amplitude mode frequency. We identify these two excitations with the second (first) breather of the sine-Gordon theory, correspondingly. In contrast to higher-dimensional systems, the amplitude and bond order fluctuations are found to carry significant spectral weight in the quasi-1D limit.

DOI: 10.1103/PhysRevLett.126.227201

Introduction.—The phenomenon of spontaneous symmetry breaking (SSB) represents one of the key notions in modern physics. For a continuous global symmetry, SSB is expected to generate two types of collective excitations—Goldstone modes, describing transverse or phase fluctuations of the order parameter, and Higgs modes, which describe its longitudinal or amplitude fluctuations. In contrast to the gapless Goldstone excitation, which is commonly observed in a variety of condensed matter systems (e.g., magnons in magnetically ordered materials), the observation of the amplitude (longitudinal) mode is more challenging. It is complicated by its intrinsically finite lifetime—an amplitude-mode excitation is allowed to decay into a pair of Goldstone excitations which leads to a strong damping of this excitation. By now several successful experimental sightings of the amplitude mode have been reported in the dimerized [1] and quasi-one-dimensional (1D) quantum magnets $KCuF_3$ [2,3], $BaCu_2Si_2O_7$ [4], Ising-like spin chains $SrCo_2V_2O$ and Yb_2Pt_2Pb [5,6] as well as in superconducting settings [7,8].

The amplitude mode is a well-defined excitation when its lifetime is long, which requires suppression of the decays into Goldstone modes, the spin waves. Theoretically, such suppression requires weakening of the long range magnetic order, the magnitude of which determines the spectral weight of the spin waves. Two ways to achieve this have been proposed, through (a) quantum critical points (QCPs) [9–12] and (b) dimensional crossover towards one dimension (1D) [13–16]. The first strategy was recently verified via quantum Monte Carlo model simulations in a dimerized antiferromagnet [17–19] and superconductor-insulator transition [20].

In this Letter, we explore the second, quasi-1D approach. It has long been proposed that a stable longitudinal model shall arise in weakly coupled spin chains [14–16]. It should be noted that this 1D critical point is strongly different from the O(3) QCP one due to the extreme spatial anisotropy of spin correlations. At the critical point, which corresponds to the limit of decoupled spin chains, excitations propagate only along chains. This feature, combined with unique properties of the spin-1/2 Heisenberg chain, imbues the ordered phase of weakly coupled spin-1/2 chains with the spinon confinement physics which is absent in the spatially isotropic magnetically ordered phase with spontaneously broken O(3) symmetry.

To study the excitation spectrum of the quasi-1D spin system, we utilize quantum Monte Carlo (QMC) simulations and stochastic analytic continuation (SAC) [21–23] to compute the spectral information of weakly coupled Heisenberg spin-1/2 chains. The predicted amplitude modes are directly observed in the numerics as the interchain interaction is reduced towards zero, and the dispersions of all low-energy modes agree nicely with analytic predictions. More importantly, we find that the

amplitude mode in quasi-1D systems exhibits two novel features. First, in contrast with higher-dimensional magnets, the amplitude mode in quasi-1D systems is characterized by a spectral weight significantly stronger than the continuum, making it highly visible and easy to detect. Second, we find that a quasi-1D spin-1/2 magnet contains *three*, instead of two, low-energy modes. In addition to the phase and amplitude modes, visible in the dynamic spin correlation functions, an additional scalar mode emerges in the dynamic *bond correlation* function. Similar to the amplitude mode, this scalar mode is singletlike but exhibits different frequency and momentum dependence.

In higher dimensions, it has been known that the scalar susceptibility serves as a great tool for probing fluctuations in the singlet channel [10] and has been widely used in numerical studies of dimerized antiferromagnets [17–19]. Inside the ordered SSB phase scalar fluctuations overlap with the amplitude ones but with much suppressed damping, and the scalar susceptibility exhibits a sharp peak at the amplitude mode frequency [11]. The quasi-1D limit is different. We show that in contrast to the amplitude mode which corresponds to the "second breather" in the effective sine-Gordon description of the ordered quasi-1D magnet, the scalar mode is represented by the "first breather," an excitation with smaller frequency which is probed via the dynamic bond-bond correlation function.

The model and the QMC method.—The geometry of the problem is shown in Fig. 1. The Hamiltonian reads

$$H = J\sum_{\langle i,j\rangle_x} \mathbf{S}_i \cdot \mathbf{S}_j + J_\perp \sum_{\langle i,j\rangle_y} \mathbf{S}_i \cdot \mathbf{S}_j - h\sum_i (-1)^i S_i^z, \quad (1)$$

where $\mathbf{S}_i = (S_i^x, S_i^y, S_i^z)$ denotes the spin-1/2 operator on site i and J ($J_\perp$) is the nearest-neighbor Heisenberg exchange along the x (y) direction. We set $J = 1$ and introduce ratio $g = J_\perp/J$ to control the crossover from decoupled 1D chains, $g = 0$, to the isotropic 2D square lattice, $g = 1$. The last term represents the staggered pinning field h, which explicitly breaks the spin-rotational symmetry.

In our QMC simulations the following three correlation functions are measured: the transverse spin correlation function $G_{S^x}(\mathbf{q},\tau) = (1/L^2)\sum_{i,j} e^{-i\mathbf{q}\cdot(\mathbf{r}_i-\mathbf{r}_j)}\langle S_i^x(\tau)S_j^x(0)\rangle$, the similarly defined longitudinal S^z correlation function $G_{S^z}(\mathbf{q},\tau)$, and the bond correlation $G_B(\mathbf{q},\tau) = (1/L^2)\sum_{i,j} e^{-i\mathbf{q}\cdot(\mathbf{r}_i-\mathbf{r}_j)}\langle B_j(\tau)B_i(0)\rangle$. Here $B_i = \mathbf{S}_i \cdot \mathbf{S}_{i+\hat{x}}$ is a spin singlet bond operator (dimerization order parameter) defined on a nearest-neighbor bond of the spin chain, L is the linear system size and $\tau \in [0,\beta]$ is the imaginary time. In the ordered SSB ground state with finite $\langle S^z\rangle \neq 0$ phase fluctuations (spin waves) are probed by G_{S^x}, G_{S^z} measures the amplitude fluctuations, and the scalar correlation function G_B probes correlations between bonds (energy density) [17–19].

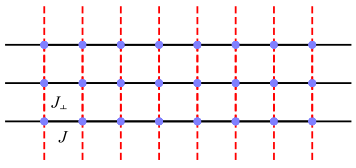

FIG. 1. Coupled antiferromagnetic Heisenberg spin chains with nearest-neighbor spin exchange J (black solid line) and $J_\perp$ (red dashed line).

It is important to notice that the SSB ground state is not possible in the QMC simulation on a finite $L \times L$ system and at finite inverse temperature β. Therefore, in the QMC with $h = 0$, there is no distinction between the phase and amplitude correlation functions, $G_{S^x}(\mathbf{q},\tau) = G_{S^z}(\mathbf{q},\tau)$. Finite $h \neq 0$ breaks spin-rotational symmetry and allows one to probe the amplitude mode by measuring G_{S^z}. It also induces the h-dependent gap in the phase mode in G_{S^x} [24–26].

In order to access real-time quantum dynamics and obtain the real-frequency spectral function $A(\mathbf{q},\omega)$ from the imaginary-time correlation $G(\mathbf{q},\tau)$, $G(\mathbf{q},\tau) = (1/\pi)\int_0^\infty d\omega A(\mathbf{q},\omega)(e^{-\tau\omega} + e^{-(\beta-\tau)\omega})$, we employ the stochastic analytic continuation (SAC). This technique, details of which are described in Refs. [27–30] and the Supplemental Material (SM) [31], has been successfully applied to a broad range of quantum magnets [32,37–45].

Analytical theory.—At small $g = J_\perp/J \ll 1$, a variety of exact (Bethe ansatz) and nonperturbative approaches (bosonization and renormalization group) are available. In the $g = 0$ limit elementary excitations of the spin chain are right- and left-moving spinons, neutral spin-1/2 fermions $\psi_{R/L,s}$, which encode an extended $\mathrm{SU}(2)_R \times \mathrm{SU}(2)_L$ symmetry of chiral rotations at low energies. The staggered part of the lattice spin operator is expressed via spinons as $S_i^a \sim (-1)^i \psi_{Rs}^\dagger \sigma_{ss'}^a \psi_{Ls'} + \mathrm{H.c.}$, where σ^a is the Pauli matrix. The singlet bond operator is staggered as well, $B_i \sim (-1)^i \psi_{Rs}^\dagger \psi_{Ls} + \mathrm{H.c.}$. These expressions define physical response functions G_{S^a} and G_B of the chain. When continued to the real frequency, the response is given by the triplet and singlet spinon continua, correspondingly.

Interchain interaction, $g \neq 0$, causes *confinement of spinons*, binding them in triplet and singlet pairs. This is easiest seen with the help of the chain mean-field theory [15,16,33,34] which maps the problem to the 1D sine-Gordon model by approximating the $J_\perp$ term in Eq. (1) by the interchain staggered field $2J_\perp m_0 \sum_i (-1)^i S_i^z$ with the self-consistently determined staggered magnetic order $m_0 = (-1)^i\langle S_i^z\rangle$ along the z axis [31]. This mean field breaks spin rotational symmetry of the problem (with $h = 0$). The excitation spectrum of the sine-Gordon model consists of solitons and antisolitons of mass Δ_0, which describe transverse spin excitations, and their bound states, breathers. The amplitude mode, which within the

low-energy mapping to the sine-Gordon model is represented by $S^z \sim \cos(\Phi/2)$, is described by the *second* breather, of mass $\sqrt{3}\Delta_0$. The singlet mode, which is represented as $B \sim \sin(\Phi/2)$, is instead described by the *first* breather, of mass Δ_0, see Ref. [31] and Refs. [16,34]. This brief description shows that in the system of weakly coupled spin-1/2 chains the amplitude, S^z, and the scalar, B, modes are distinct and *independent* excitations.

Detailed calculation of spin and bond susceptibilities are presented in the SM [31]. The dispersions of the phase (S^x and S^y), amplitude (S^z), and bond (B) modes near $k_x = \pi$ are

$$\omega_{S^x} = \omega_{S^y} = \Delta_0 \sqrt{1 + b_h + \cos k_y + \frac{v^2 (k_x - \pi)^2}{\Delta_0^2}} \quad (2)$$

$$\omega_{S^z} = \Delta_0 \sqrt{3(1+b_h) + \frac{Z_2}{Z_1} \cos k_y + \frac{v^2 (k_x - \pi)^2}{\Delta_0^2}} \quad (3)$$

$$\omega_B = \Delta_0 \sqrt{1 + b_h + \frac{v^2 (k_x - \pi)^2}{\Delta_0^2}}. \quad (4)$$

Here k_x (k_y) is the momentum along the chain (transverse to the chain) and b_h is a dimensionless parameter describing the effect of the external staggered field h, Eq. (S25). At $h = 0$, b_h vanishes and our equations for ω_{S^x} and ω_{S^z} recover the corresponding formulae in Ref. [34]. The velocity v is $\pi J/2$ and the ratio $Z_2/Z_1 \approx 0.491309$.

Note that in addition to having a different mass, the dispersion of the bond mode is different from the amplitude one as well. It propagates along the chain with the same velocity v as spin fluctuations but is essentially dispersionless in the transverse k_y direction, see Ref. [31].

Numerical results.—In Fig. 2, we present numerical results of spectral functions for spin-spin and bond-bond correlations, with and without the pinning field h and compare them with the dispersions (cyan lines) obtained from analytic theory Eqs. (2)–(4). From the top to bottom row, the values of g are 0.5, 0.1, and 0.05, reflecting the dimensional crossover from 2D to quasi-1D. The system has periodic boundary condition $L \times L$ with $L = 36$. The QMC calculations are carried out at inverse temperature $\beta = 4L$. The spectra are plotted along the high-symmetry path indicated in the BZ in panel Fig. 2(c). The first (last) two columns of Fig. 2 are measured in the absence (presence) of the staggered field h.

Key differences between the 2D [$g = 0.5$, Figs. 2(a)–2(d)] and quasi-1D regimes [$g = 0.1$ for Figs. 2(e)–2(h) and $g = 0.05$ for Figs. 2(j)–2(l)] are easily seen. For $g = 0.5$ the phase mode is clearly visible in panels (a) and (c) while the amplitude and scalar fluctuations (d) and (b) exhibit only an overdamped multimagnon continuum without any sharp modes, as expected [13,14]. As the system moves towards 1D ($g = 0.1$ and 0.05), the single magnon mode remains sharp and becomes more 1D-like (i.e., less dispersive along the interchain $M - X_1$ direction). At the same time, the spectral weight in the bond [Figs. 2(f) and 2(j)] and amplitude [Figs. 2(h) and 2(i)] sectors shifts down in energy, resulting in the emergence of the two low energy peaks in corresponding spectral densities.

Let us investigate these differences closer. The first column in Fig. 2 shows A_{S^x} at $h = 0$. Note that simulations

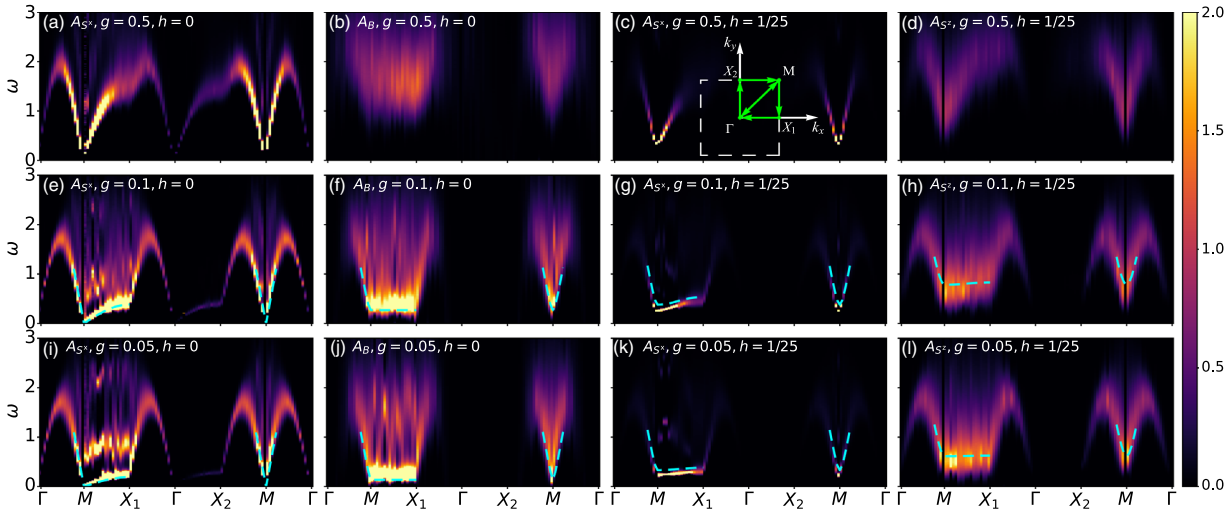

FIG. 2. Spectral functions obtained from QMC SAC. (a), (e), (i) and (b), (f), (j) show the spectra function of spin and bond operators, respectively, $A_{S^x}(\mathbf{q}, \omega)$ and $A_B(\mathbf{q}, \omega)$, without the field, $h = 0$, at different values of $g = J/J_\perp$, with the system size is $L = 36$, and inverse temperature $\beta = 4L$. The dashed cyan curves in (e), (i) and (f), (j) are analytical dispersions in Eqs. (2) and (4) with $b_h = 0$. (c), (g), (k) and (d), (h), (l) show the phase mode spectra $A_{S^x}(\mathbf{q}, \omega)$ and amplitude mode spectra $A_{S^z}(\mathbf{q}, \omega)$ measured in the presence of a weak staggered field $h = 1/25$, with system size $L = 36$ and inverse temperature $\beta = 4L$. The dashed cyan curves in (g), (k) and (h), (l) are analytical dispersions in Eqs. (2) and (3) with finite b_h.

in finite size and temperature system are necessarily done in the symmetric phase with three components of spin susceptibility degenerate $A_{S^x} = A_{S^y} = A_{S^z}$. The minimal spin excitation energy, measured at the M point (π, π), is small but finite. At $g = 0.05$ it is about 0.004. The dispersion of the lowest energy branch is well described by the pole of the RPA susceptibility Eq. (S35). Notice that in this magnetically disordered phase the gap is $\Delta^2 - 2Z_1 J_\perp > 0$, as discussed above. It vanishes only in the thermodynamic limit $L = \infty$ when the SSB takes place and the spin rotational symmetry gets broken, resulting in different dispersion relations for transverse, Eq. (2), and longitudinal, Eq. (3), modes (with $b_h = 0$).

We also observe noticeable spectral intensity at higher energy, $\omega \approx 0.6$–0.7, in Figs. 2(e) and 2(i). We assign this to the second breather of the sine-Gordon + RPA theory, Eq. (S36), with the mass $\sqrt{3}\Delta$ [31]. Naturally, this feature is absent in the 2D limit, Fig. 2(a), where our quasi-1D arguments do not apply. This interpretation is further supported by the data for bond spectral function A_B, presented in the second column of Fig. 2. Here, one observes a pronounced difference between the 2D, $g = 0.5$, and 1D limits, $g = 0.05$ and 0.1: the broad and overdamped multiparticle continuum evolves into a very structured one with a sharp particlelike peak at the lowest energy for small-g cases, in Figs. 2(f) and 2(j). This is the first breather of the sine-Gordon model, describing the scalar bond (staggered dimerization) mode, with mass Δ, of weakly coupled spin chains, as described below Eq. (4). As explained in the SM [31], its dispersion along k_y is negligible while that along k_x matches Eq. (4) (with $b_h = 0$) very well.

Taken together, our data lend strong support to the description of the spin system in terms of *confined* spinon pairs. The spin susceptibility is described by the triplet of bound spinons and its internal excited state (the second breather) while the scalar susceptibility is represented by bound singlet pairs of spinons.

To differentiate between the transverse and longitudinal fluctuations we next turn on the staggered field $h \neq 0$ along the z axis. The corresponding QMC data are represented by the last two columns of Fig. 2. Now $A_{S^x} = A_{S^y}$ measures the phase fluctuations of the order parameter (the third column), which are gapped stronger by the finite h, while A_{S^z} gives the amplitude fluctuations (the last column).

To illustrate the emergence of the amplitude and scalar modes we plot in Fig. 3 the frequency dependence of these two spectra at different values of g at the wave vector $\mathbf{k} = (\pi, \pi/2)$. In 2D ($g = 0.5$), both spectra exhibit a continuum background from multimagnon excitations. As g gets smaller, a peak emerges in the spectral function and becomes sharper as g becomes smaller. It is seen that for the same value of g the peak in A_B is more narrow and occurs at a lower frequency than that in A_{S^z}. The larger linewidth of the amplitude mode is due to the stronger

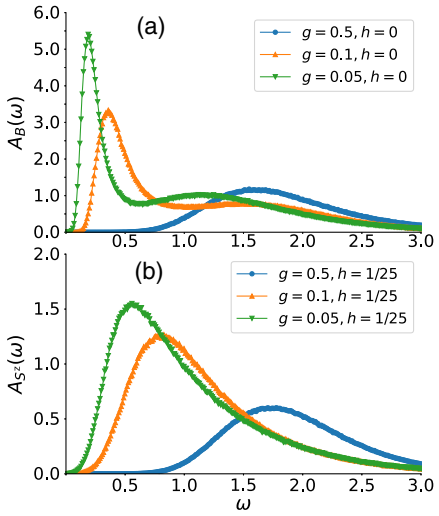

FIG. 3. Frequency dependence of the spectral functions at $\mathbf{k} = (\pi, \pi/2)$ for (a) the bond-bond correlation at $h = 0$ and (b) the amplitude mode at $h = 1/25$.

damping it experiences due to decays into the low energy phase fluctuations, in comparison with the bond correlation function [10], while the peak's maxima difference is a unique property of quasi-1D system as Eqs. (3) and (4) show.

In Fig. 4, we present the finite-size analysis and extrapolate the peak frequency of each mode to the thermodynamic limit. Here, we focus on the momentum point $\mathbf{k} = (\pi, \pi/2)$, at which the interchain dispersion vanishes within the RPA approximation, and the frequency of a mode is obtained by fitting the correlation function to an exponential function of the imaginary time $\propto e^{-\omega\tau}$ (several representative cases of such fitting are presented in SM [31]). Given the square-root form of dispersions (2),

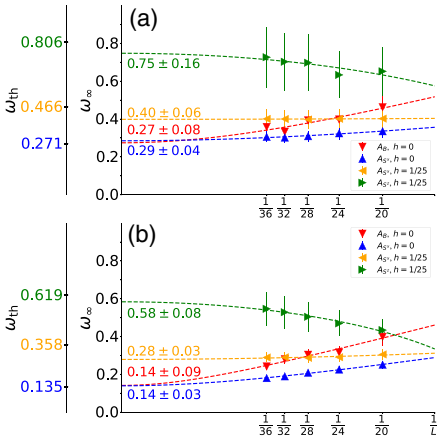

FIG. 4. Finite-size analysis for (a) $g = 0.1$ and (b) $g = 0.05$ at the momentum point $\mathbf{k} = (\pi, \pi/2)$. The vertical ω_∞ axis shows extrapolation of the numerical data to the $L = \infty$ limit. Values on the left vertical ω_{th} axis mark analytical predictions for the peak frequencies of different modes. See main text for details.

(3), and (4), we take the following functional form for the extrapolation to infinite size $\omega_L = \sqrt{\omega_\infty^2 + L_0^2/L^2}$, where ω_∞ and L_0 are fitting parameters. The results for so obtained ω_∞ are presented to the right of the ω_∞ axis in Fig. 4. As discussed above, without the staggered field the lowest energy peak in $A_{S^x}(h=0)$ describes coherent threefold degenerate mode ω_{S^x}. At finite $h = 1/25$, the degeneracy is removed and ω_{S^x} and ω_{S^z} scale to different limits. Within the sine-Gordon description $\omega_{S^z}/\omega_{S^x} = \sqrt{3}$, see Eqs. (2) and (3). Figure 4 shows that this ratio extrapolates to 1.8 for $g = 0.1$ and to 2.0 for $g = 0.05$ at $L = \infty$. The ω_{th} axis in Fig. 4 shows analytical predictions for $\omega_{S^x}, \omega_{S^z}$, which are calculated as functions of g and h, without any adjustable parameters, in the SM [31]. This parameter-free comparison is seen to work reasonably well. In addition, in agreement with analytical predictions, Fig. 4 shows that for $h = 0$, ω_{S^x} and ω_B extrapolate to the same limit, just as Eqs. (2) and (4) with $b_h = 0$ require.

O. A. S. thanks Sasha Chernyshev for insightful discussions. C. K. Z., Z. Y., and Z. Y. M. acknowledge the support from the RGC of Hong Kong SAR China (Grants No. 17303019, No. 17301420, and No. AoE/P-701/20), and MOST through the National Key Research and Development Program (2016YFA0300502). O. A. S. was supported by the NSF CMMT program under Grant No. DMR-1928919. H. Q. W. is thankful for support from NSFC-11804401 and the Fundamental Research Funds for the Central Universities (19lgpy266). We thank the Computational Initiative at the Faculty of Science and the Information Technology Services at the University of Hong Kong and the National Supercomputer Centers in Guangzhou and Beijing PARATERA Tech CO., Ltd. for their technical support and providing generous HPC resources that have contributed to the research results reported within this paper. This research was initiated at the Aspen Center for Physics, supported by NSF PHY-1066293.

*sunkai@umich.edu
†starykh@physics.utah.edu
‡zymeng@hku.hk

[1] P. Merchant, B. Normand, K. W. Krämer, M. Boehm, D. F. McMorrow, and C. Rüegg, Nat. Phys. **10**, 373 (2014).
[2] B. Lake, D. A. Tennant, and S. E. Nagler, Phys. Rev. Lett. **85**, 832 (2000).
[3] B. Lake, D. A. Tennant, and S. E. Nagler, Phys. Rev. B **71**, 134412 (2005).
[4] A. Zheludev, M. Kenzelmann, S. Raymond, T. Masuda, K. Uchinokura, and S.-H. Lee, Phys. Rev. B **65**, 014402 (2001).
[5] A. K. Bera, B. Lake, F. H. L. Essler, L. Vanderstraeten, C. Hubig, U. Schollwöck, A. T. M. N. Islam, A. Schneidewind, and D. L. Quintero-Castro, Phys. Rev. B **96**, 054423 (2017).
[6] W. J. Gannon, I. A. Zaliznyak, L. S. Wu, A. E. Feiguin, A. M. Tsvelik, F. Demmel, Y. Qiu, J. R. D. Copley, M. S. Kim, and M. C. Aronson, Nat. Commun. **10**, 1123 (2019).
[7] D. Sherman, U. S. Pracht, B. Gorshunov, S. Poran, J. Jesudasan, M. Chand, P. Raychaudhuri, M. Swanson, N. Trivedi, A. Auerbach, M. Scheffler, A. Frydman, and M. Dressel, Nat. Phys. **11**, 188 (2015).
[8] R. Shimano and N. Tsuji, Annu. Rev. Condens. Matter Phys. **11**, 103 (2020).
[9] S. Sachdev, Phys. Rev. B **59**, 14054 (1999).
[10] D. Podolsky, A. Auerbach, and D. P. Arovas, Phys. Rev. B **84**, 174522 (2011).
[11] S. Gazit, D. Podolsky, and A. Auerbach, Phys. Rev. Lett. **110**, 140401 (2013).
[12] H. D. Scammell and O. P. Sushkov, arXiv:1705.09007.
[13] C. M. Canali and S. M. Girvin, Phys. Rev. B **45**, 7127 (1992).
[14] I. Affleck and G. F. Wellman, Phys. Rev. B **46**, 8934 (1992).
[15] H. J. Schulz, Phys. Rev. Lett. **77**, 2790 (1996).
[16] F. H. L. Essler, A. M. Tsvelik, and G. Delfino, Phys. Rev. B **56**, 11001 (1997).
[17] M. Lohöfer, T. Coletta, D. G. Joshi, F. F. Assaad, M. Vojta, S. Wessel, and F. Mila, Phys. Rev. B **92**, 245137 (2015).
[18] Y. Q. Qin, B. Normand, A. W. Sandvik, and Z. Y. Meng, Phys. Rev. Lett. **118**, 147207 (2017).
[19] M. Lohöfer and S. Wessel, Phys. Rev. Lett. **118**, 147206 (2017).
[20] M. Swanson, Y. L. Loh, M. Randeria, and N. Trivedi, Phys. Rev. X **4**, 021007 (2014).
[21] A. W. Sandvik, in *AIP Conference Proceedings* (AIP, New York, 2010), Vol. 1297, pp. 135–338.
[22] O. F. Syljuåsen and A. W. Sandvik, Phys. Rev. E **66**, 046701 (2002).
[23] F. Alet, S. Wessel, and M. Troyer, Phys. Rev. E **71**, 036706 (2005).
[24] I. Affleck and M. Oshikawa, Phys. Rev. B **60**, 1038 (1999).
[25] F. H. L. Essler, A. Furusaki, and T. Hikihara, Phys. Rev. B **68**, 064410 (2003).
[26] I. Kuzmenko and F. H. L. Essler, Phys. Rev. B **79**, 024402 (2009).
[27] A. W. Sandvik, Phys. Rev. B **57**, 10287 (1998).
[28] K. S. D. Beach, arXiv:cond-mat/0403055.
[29] A. W. Sandvik, Phys. Rev. E **94**, 063308 (2016).
[30] A. W. Sandvik, J. Phys. A **25**, 3667 (1992).
[31] See Supplemental Material at http://link.aps.org/supplemental/10.1103/PhysRevLett.126.227201 for details of the QMC-SAC implementation of the quasi-1D quantum magnet, the QMC measurement of dynamic bond correlation function and the detailed discussion on the analytical calculation of the excitation spectra, which includes Refs. [16,18,19,21–24,29,32–36].
[32] H. Shao, Y. Q. Qin, S. Capponi, S. Chesi, Z. Y. Meng, and A. W. Sandvik, Phys. Rev. X **7**, 041072 (2017).
[33] A. W. Sandvik, Phys. Rev. Lett. **83**, 3069 (1999).
[34] F. H. L. Essler and R. M. Konik, in *From Fields to Strings: Circumnavigating Theoretical Physics: Ian Kogan Memorial Collection* (in 3 Vols), edited by M. Shifman (World Scientific Publishing Co. Pte. Ltd, Singapore, 2005), Vol. 1, pp. 684–830.

[35] S. Lukyanov and A. Zamolodchikov, Nucl. Phys. **B493**, 571 (1997).
[36] T. Hikihara and O. A. Starykh, Phys. Rev. B **81**, 064432 (2010).
[37] Y. Xu, Z. Xiong, H.-Q. Wu, and D.-X. Yao, Phys. Rev. B **99**, 085112 (2019).
[38] G.-Y. Sun, Y.-C. Wang, C. Fang, Y. Qi, M. Cheng, and Z. Y. Meng, Phys. Rev. Lett. **121**, 077201 (2018).
[39] N. Ma, G.-Y. Sun, Y.-Z. You, C. Xu, A. Vishwanath, A. W. Sandvik, and Z. Y. Meng, Phys. Rev. B **98**, 174421 (2018).
[40] C.-J. Huang, Y. Deng, Y. Wan, and Z. Y. Meng, Phys. Rev. Lett. **120**, 167202 (2018).
[41] N. Ma, Y.-Z. You, and Z. Y. Meng, Phys. Rev. Lett. **122**, 175701 (2019).
[42] Z. Yan, Y.-C. Wang, N. Ma, Y. Qi, and Z. Y. Meng, npj Quantum Mater. **6**, 39 (2021).
[43] Y.-C. Wang, M. Cheng, W. Witczak-Krempa, and Z. Y. Meng, arXiv:2005.07337.
[44] Z. Hu, Z. Ma, Y.-D. Liao, H. Li, C. Ma, Y. Cui, Y. Shangguan, Z. Huang, Y. Qi, W. Li, Z. Y. Meng, J. Wen, and W. Yu, Nat. Commun. **11**, 5631 (2020).
[45] Y.-C. Wang, Z. Yan, C. Wang, Y. Qi, and Z. Y. Meng, Phys. Rev. B **103**, 014408 (2021).